RSC Advances

PAPER

View Article Online
View Journal | View Issue

Cite this: *RSC Adv.*, 2019, **9**, 31013

Synthesis of silver particles stabilized by a bifunctional SiH_x–NH_y–PMHS oligomer as recyclable nanocatalysts for the catalytic reduction of 4-nitrophenol†

Zhen Wang,[ab] Shun Yao,[a] Shaofei Pan,[a] Jian Su,[a] Changqing Fang, *[a] Xianliang Hou[a] and Mei Zhan[b]

Bifunctional oligomers with both reducing and stabilizing functionalities were prepared and successfully applied to the preparation of silver colloids of around 2 nm size without employing a strong stabilizer such as S and P, which was quite difficult to achieve. Transmission electron microscopy (TEM) and dynamic light scattering (DLS) were performed to determine the morphology and particle size of the Ag colloids. UV-vis spectroscopy and X-ray absorption spectroscopy (XAS) were implemented to investigate the oxidation state of the Ag colloids. Synthesis parameters such as the density control of the ligating functionalities, the propinquity of the reducing and stabilizing groups, the extent of ligand stabilization and the reducing rates were found to have important effects on the formation and stabilization of Ag colloids. The as-synthesized Ag colloids were very stable even after being deposited on silica; then, they were subjected to calcination to get rid of the organics, which afforded Ag NPs (1.9–3.5 nm) on silica with narrow size distribution. These Ag NPs performed excellently in catalytic 4-nitrophenol reduction with conversion of up to 98% within 10 min. Furthermore, the Ag nanoparticles were quite stable and exhibited excellent reusability for seven successive reaction cycles without obvious decay. The straightforward synthesis of the ultra-small and stable Ag NPs has the potential for applications in the synthesis of other supported late transition metals.

Received 23rd June 2019
Accepted 28th August 2019

DOI: 10.1039/c9ra04711e

rsc.li/rsc-advances

Introduction

Nanoparticles of noble metals, especially metal nanoparticles in the quantum-size domain, have attracted tremendous attention due to their extensive applications in electronics, optics, catalysis, and biomedical and environmental fields.[1–3] Silver nanoparticles have been widely studied due to their attractive spectrum of physical properties and their significant potential for selective activity in a very wide range of applications including antimicrobial agents, wastewater purification, electronics, and biological sensing and imaging.[4–9]

Among these applications, the employment of silver NPs in sewage treatment is of great significance due to the intrinsic electronic properties and particular catalytic performance. For example, 4-nitrophenol (4-NP) is one of the most toxic pollutants that exists widely in both industrial and agriculture effluents such as petrochemicals and pharmaceuticals.[10] It is listed as a "priority pollutant" since it can hardly be removed by natural degradation and is genotoxic and carcinogenic to animals and humans.[11,12] The catalytic reduction of 4-NP over noble-metal NPs has been demonstrated to be an efficient and eco-friendly procedure for producing 4-aminophenol (4-AP), which is an important intermediate for fine chemicals such as synthetic dyes, pharmaceuticals and pesticides.[10,13] Therefore, the reduction of 4-NP to 4-AP was chosen as a model reaction to quantitatively evaluate the catalytic properties and consider pollutant treatment and green regeneration.[14,15]

The intrinsic properties of catalytic silver nanoparticles are predominantly determined by their size, shape, structure, composition and crystallinity. However, silver NPs are thermodynamically unstable and are inclined to agglomerate to minimize the surface energy, resulting in a significant decrease in catalytic activity. Colloidal silver particles of less than 2 nm size have shown many extraordinary properties since their size is fairly close to the Fermi wavelength. It has been demonstrated that there exists a strong size effect on the catalytic performance in this range.[16–19] Jiang[20] investigated the catalytic oxidation of CO on the Ag_{38} cluster supported by graphdiyne and provided intensive understanding of its high activity originating from the

[a]*Faculty of Printing, Packaging and Digital Media Technology, Xi'an University of Technology, Xi'an, Shaanxi 710048, P. R. China. E-mail: fcqxaut@163.com*

[b]*State Key Laboratory of Solidification Processing, Northwestern Polytechnical University, Xi'an 710072, P. R. China*

† Electronic supplementary information (ESI) available: NMR spectra of SiH_x–NH_y–PMHS, XPS spectra and STEM images of Ag/SiO_2-1 before and after the reaction. See DOI: 10.1039/c9ra04711e

intrinsic activity of the Ag_{38} cluster. Zamborini and co-workers addressed the size-dependent electrochemical oxidation of silver nanoparticles as a function of particle size.[21] In view of the strong correlation between stability, particle size and catalytic properties, great efforts have been made to design strategies to prepare small silver colloids, especially those less than 2 nm in size.

The concept of stabilizing silver nanoparticles is one of the potential strategies for conquering the aggregation problem. In most cases, stabilized nanoparticles are coordinated with strong surfactants to prevent agglomeration and they might show specific surface properties;[22] therefore, the selection of a stabilizer is crucial. Assuming that the stabilizer interacts weakly with Ag, the Ag atoms will migrate to form large Ag particles. Likewise, if the stabilizer interacts strongly with Ag, it could alter the surface nature of the particles so as to affect the catalytic performance significantly. Ideally, it is desirable to develop synthetic strategies to synthesize silver nanoparticles, which provide flexibility for functionalizing the nanoparticles according to the need. Many reports have shown that bifunctional stabilizers have been applied successfully in many cases such as polyoxometalates,[23] dithiocarboxylates,[24] dithiocarbamates,[25] mercaptosuccinic acid,[26] 2-mercaptopropionic acid,[27] mercaptocarbonyl compounds[28] and ethylenediamine tetraacetate.[29] As for the bifunctional stabilizers, one functional group is ligated to the silver particle, and the other one offers a charged layer that can stabilize the particles and prevent them from aggregating by charge–charge repulsion. Ultimately, we would like to synthesize stable silver particles with high catalytic activity, but there are two crucial problems worth considering. First, both sulfur and phosphorus have strong chemical interactions with Ag, which can influence the chemical properties of the surface atoms. Thus, the activation of silver catalyst often need harsh treatment to remove the stabilizer which will lead to notable coarsening of the silver particles. Second, it is accepted that residual S or P can poison the Ag catalysts in the presence of stable sulfates or phosphates.[30,31] Thus, there is a strong potential to identify bifunctional stabilizers that on the one hand interact more weakly with Ag as compared with S and P and on the other hand can ligate and stabilize silver nanoparticles with narrow size distribution.

Herein, bifunctional SiH_x–NH_y–PMHS oligomers were synthesized and used to successfully prepare stable and uniform silver colloids smaller than 2 nm without using a strong stabilizer such as S and P, which is known to be difficult to accomplish. Significantly, by designing both reducing and stabilizing groups in a single oligomer, their interactions with the silver precursor and the proximity of the functional groups could be manipulated, so that the reduction and nucleation processes of silver nanoparticles could be controlled at the atomic level as well as in the subsequent stabilization process. We designed and synthesized a functionalized oligomer as a stabilizer containing two types of groups for the fabrication of colloidal Ag with the size of around 2 nm. The –SiH groups functioned as the reducing agent, the –NH groups were coordinated to the surface Ag atoms, and the particles were stabilized from agglomeration. Besides, the ratio of the two ligands could be adjusted by a hydrolytic process. Furthermore, another transition metal could be incorporated into the resulting colloids, which could be potentially used to design and synthesize binary noble catalysts. Subsequently, the preparation process was monitored by recording the NMR spectra in solution, and we obtained deep insights into the synthesis parameters that determined the morphology of silver colloids. We confirmed the essential proximal location of the –NH groups and the reducing SiH ligand; we also established that the density of the ligating groups, the proximity of the ligating and reducing groups and the rates of reduction have a strong effect on the particle sizes of silver colloids. The as-synthesized Ag colloids were very stable even after being deposited on silica; subsequently, they were calcined to burn the organics in He and O_3 atmospheres, which afforded Ag NPs (1.9–3.5 nm) on silica with narrow size distribution. Finally, the reduction of 4-nitrophenol to 4-aminophenol with excess $NaBH_4$ was employed as a probe reaction to screen the activities of these AgNPs. The reaction kinetics were investigated by monitoring the time-dependent conversion of 4-nitrophenol in the system. Moreover, these catalysts could be recycled for seven successive cycles without obvious decay, indicating that this is a promising method for fabricating stable silver catalysts for 4-nitrophenol treatment in large-scale processes. This novel and facile method provides potential applications for the design of heterogeneous catalysts and can furnish grounds for fundamental catalysis research.

Experimental

Materials

All the reagents and solvents were purchased from commercial companies and were used as received without further purification. Poly(methylhydro)siloxanes (PMHS **I**, 1700–3200 g mol^{-1}), palladium hydroxide on carbon (30 wt% loading), silver acetate (99.0%), 4-nitrophenol (≥99.0%), sodium borohydride (≥99.0%), toluene (anhydrous, 99.8%), tetrahydrofuran (99.9%), ethyl ether (≥99.0%), calcium sulfate (drierite, 8 mesh), triethylsilane (99%) were purchased from Sigma-Aldrich. *N*-Methyl-aza-2,2,4-trimethylsilacyclopentane was purchased from Gelest. Celite and sodium sulfate (≥99.0%) were purchased from EMD Chemicals. Experiments referring to compounds **II** and **III** were performed under N_2 protection either in an N_2 glovebox or using a Schlenk line.

Synthesis of bifunctional oligomer SiH_x–NH_y–PMHS

Scheme 1 shows the steps in the synthesis of the bifunctional amino hydrosiloxane SiH_x–NH_y–PMHS. First, 0.64 mL PMHS **I** containing 10 mmol SiH groups was added to a Schlenk flask that was preloaded with 20 mL THF. Quantitative H_2O (90 mg, 180 mg, 300 mg) was added to partially or totally oxidize the –SiH groups to –SiOH groups in the presence of Pearlman's catalyst to form SiH_x–$SiOH_y$–PMHS (**II** or **III**). The reaction was monitored by the H_2 evolution. Once the H_2 evolution ceased, the remaining mixture was dried thoroughly with sodium sulfate. Column chromatography was performed to remove the

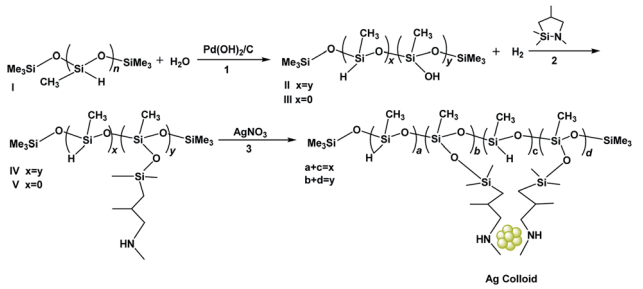

Scheme 1 Synthesis of the bifunctional SiH_x–NH_y–PMHS oligomer for Ag colloid preparation.

Pearlman's catalyst, in which sandwiched Celite and Drierite were layered using diethyl ether as the eluent. After that, the –SiOH groups of synthesized **II** or **III** were quantitatively reacted with evaporation to generate the desired SiH_x–NH_y–PMHS oligomer **IV** or *N*-methyl-aza-2,2,4-trimethylsilacyclopentane under N_2 protection. The mixture was stirred for around 30 min followed by the addition of solvent **V**. The as-synthesized compounds were characterized with NMR spectra; they are shown in Fig. S1 and S2.† ^{1}H NMR (400 MHz, CDCl3) δ 0–0.015 (–Si(CH_3)$_3$, –Si(CH_3)$_2$, –SiHCH_3, –SiCH_3); 0.38 (–SiCH_2); 0.63 (–SiCH_2); 0.84 (–N*H*); 0.92 (CH_3CH–); 1.80 (CH_3C*H*–); overlapped 2.43 (–NHCH_2, –NHCH_3); 4.8(Si*H*–); 7.26 ($CDCl_3$).^{13}C NMR (100 MHz, $CDCl_3$) δ −2.64 (–Si(CH_3)$_3$); 1.09 (–SiCH_3); 1.37 (–Si(CH_3)$_2$); 20.96 (CH_3CH–); 24.55 (–SiCH_2); 29.09 (CH_3C*H*–); 36.58 (–NHCH_3); 61.64 (–NHCH_2); 77.00 ($CDCl_3$). ^{29}Si NMR (80 MHz, $CDCl_3$) δ −66.91 (–*Si*CH_3); −36.60 (–*Si*HCH_3); 6.32 (–Si(CH_3)$_3$); 7.97 (–Si(CH_3)$_2$).

Synthesis of silver colloids with as-synthesized bifunctional oligomer

Synthesis of amine-functionalized silver colloids. Quantitative SiH_x–NH_y–PMHS was dissolved in THF solution in an ice bath. Then, aliquots of 6 mM $AgNO_3$ solution in methanol were added to the vial. In these experiments, the amounts of oligomer and $AgNO_3$ added were calculated with respect to the –SiH or –NH group. When –SiH was not an internal portion of the oligomer, a mild reductant, triethylsilane, was introduced into the system. Different ratios of SiH/NH/Ag were examined, which are shown in Table 1. The total amount of the mixture was maintained at 10 mL and the silver concentration was maintained at 3 mM finally. The reaction was kept for one hour at 0 °C. Silica-supported silver nanoparticles were made by grafting Ag colloids onto Cabosil-L90 immersed in THF and then calcined in He and O_3/O_2 atmospheres in sequence at 150 °C.

Sample characterization

NMR spectra were collected with an Agilent DD2 spectrometer and the data were processed with MNova 9.0 software. The morphologies of Ag colloids were examined using the TEM model on a JEOL 2100-F transmission electron microscope. High angle annular dark-field STEM images were obtained with a field emission gun at 200 kV. Particle size distribution was analyzed by counting more than 300 particles based on the images. Dynamic light scattering spectra were obtained with Brookhaven BI9000, which could measure the hydrodynamic diameters of the Ag colloids. A Thermo ESCALAB 250Xi instrument was used to collect X-ray photoelectron spectra. It was equipped with an electron flood gun using Al Kα radiation (1486.6 eV). An HP8452 diode array spectrophotometer was used to acquire the UV-vis absorption spectra. Beamline 5-BMD was used to obtain X-ray absorption spectra in the fluorescence mode. The data were collected at a temperature of about 25 K, using a helium cryostat, in order to reduce the Debye–Waller effects. Silver foil and silver nitrate were applied as the standards. Demeter was used to analyze the XAS data.

Catalytic test of the as-synthesized catalysts

The reduction of 4-NP with excess $NaBH_4$ solution was used as a model reaction to quantitatively evaluate the catalytic activity of the silver nanocatalysts. The reaction kinetics did not depend on the concentration of the $NaBH_4$ solution. Once $NaBH_4$ was added to the 4-NP solution, the color immediately changed from light yellow to yellow-green due to the formation of 4-nitrophenolate ions in the solution. Then, the yellow-green color gradually faded over time after introducing silver nanocatalysts due to the conversion of 4-NP to 4-AP. The reduction process was monitored by UV-vis spectra collected at different time intervals.

Typically, 40 mL mixed aqueous solution containing 3 mM 4-NP and 100 mM $NaBH_4$ was prepared. Then, the Ag nanocatalyst (containing 0.005 mmol Ag) was added to the reaction with continuous stirring to form a suspension at room temperature.

Table 1 Average Ag particle size in different preparations

			Synthesis solution conditions[b]				
Sample	H_2O added[a](mg)	Amine and silane carrier	[Olig][c] (mM)	[Amine][d](mM)	Ag/SiH	T (°C)	Ag colloid diameter[e] (nm)
A	0	PMHS **I**	0.8	—	1 : 10	0	10.5 ± 3.3
B	90	SiH–NH–PMHS **V**	1.6	30	1 : 10	0	1.2 ± 0.4
C	180	Et_3SiH + NH–PMHS **IV**	0.8	30	1 : 3	0	2.5 ± 0.9
D	300	Et_3SiH + NH–PMHS **IV**	0.8	30	1 : 10	0	3.6 ± 1.5
E	90	SiH–NH–PMHS **V**	1.6	30	1 : 10	25	5.4 ± 1.94

[a] Quantitative H_2O was added to partially or totally oxidize SiH to silanols in the presence of Pearlman's catalyst. [b] N/Ag atomic ratio was 10. [c] Based on an average of 38 siloxane units per oligomer. [d] Calculated using the extent of conversion of SiH to amino units. [e] Based on 300 particles.

At appropriate time intervals, an aliquot of the reaction mixture was taken out with a syringe and filtered with membrane filters. The UV-vis absorption spectrum of the filtrate was recorded immediately. The reaction rate was measured based on the absorbance intensity of the 4-nitrophenolate ion peak at 400 nm as a function of time.

When studying the recycling of the active catalyst Ag/SiO_2-1 system, the solution obtained after the reaction was filtered with a membrane filter and the solid was washed with deionized water for several times. After that, the recovered catalyst was dried in the oven at 80 °C for the next run under the same conditions.

Results and discussion

Interaction of $AgNO_3$ with the bifunctional oligomer SiH_x–NH_y–PMHS

The resonances of the protons of the Ag colloid and the corresponding oligomers are shown in Fig. 1. The two protons of NH–CH_2– were diastereotopic and appeared as broad and multiplet peaks together with the NH–CH_3 resonance at around 2.3–2.4 ppm. Based on the integrated areas of N*H*–, NH–CH_2– and NH–CH_3, we inferred that the integration accounted for the majority of the protons associated with the amine groups in the oligomer. The existence of the –SiH groups in oligomer **IV** resulted in the immediate reduction of Ag(I) after mixing with the Ag precursor. The following remarkable changes were observed and the resonance shifted from δ 0.85 to 2.5 ppm (Fig. 1A and B). The overlapping NH–CH_2– and NH–CH_3 peaks now separated into two peaks: a relatively broader one at δ 2.38 ppm and a sharper one at δ 2.48 ppm in the resonance peaks of N*H*–, NH–CH_2– and NH–CH_3. The N*H*– peak was at 2.48 ppm. However, the addition of Et_3SiH in oligomer **V** gave rise to the reduction of Ag(I) after mixing with the Ag precursor and obvious variations in the peaks of N*H*–, NH–CH_2– and NH–CH_3. The N*H*– resonance shifted from δ 0.85 to 1.25 ppm (Fig. 1C and D). A new broad peak that appeared at 2.9 ppm (Fig. 1D) could be assigned to NH–CH_2– and NH–CH_3 of oligomer **IV**, which coordinated to Ag(I). The overall prominent shifts demonstrated that the structure was altered in oligomers **IV** and **V**. We inferred that Ag(I) was reduced by SiH and the formed compound could easily react with a neighboring N*H*– group in the form of a new silazane bond accompanied by the protonation of another amine group.[32] The proposed equations are listed below. These structural modifications gave rise to the observed spectroscopic shifts and essentially reflected the conformational changes in the oligomer.

$$-\mathrm{NHR} + \mathrm{AgNO_3} = \mathrm{Ag(NHR)NO_3} \quad (1)$$

$$2(\mathrm{NHR})\mathrm{Ag^{I}NO_3} + 2\mathrm{R_3SiH} = 2\mathrm{NHRAg^0} + 2\mathrm{R_3Si(NO_3)} + \mathrm{H_2} \quad (2)$$

$$\mathrm{R_3Si(NO_3)} + 2\mathrm{NHR_2} = \mathrm{R_3SiNR_2} + \mathrm{R_2(NH_2)^+(NO_3)^-} \quad (3)$$

Characterization of silver colloids synthesized with bifunctional oligomers

The TEM images of samples A to E are shown in Fig. 2. Not surprisingly, sample A showed large non-uniform Ag agglomerates larger than 10 nm. This is not difficult to understand since this sample was prepared without amine ligands on the backbone of the oligomer, which demonstrated that amine ligands are imperative to stabilize small Ag colloids. For sample B, the predominant Ag particles were around 1.2 nm in diameter, while for samples C and D, the Ag particles were around 2.5–3.6 nm in diameter. For sample B, it was observed that the particle size of the Ag colloids (Table 1) was smaller (compared with those for C and D) and the uniformity was much higher. The difference was that the sample B was prepared with a bifunctional oligomer possessing internal reducing (–SiH) groups and ligating (amine) groups. However, samples C and D were synthesized with oligomers containing amine groups only, and the external reducing –SiH groups were added in the

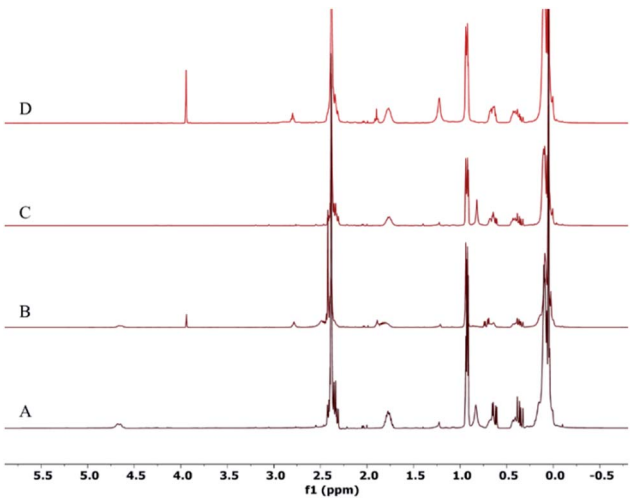

Fig. 1 ^{1}H NMR spectra of Ag colloid samples after the addition of $AgNO_3$ to SiH_x–NH_y–PMHS **IV** and **V**. (A–D) Correspond to SiH_x–NH_y–PMHS **IV**, Ag-**IV**, **V** and Ag-**V**.

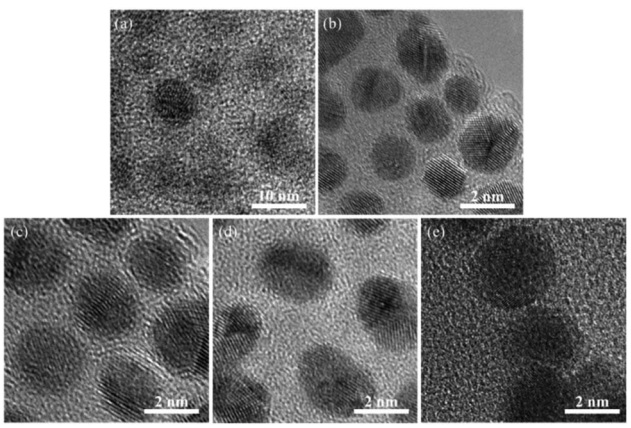

Fig. 2 TEM images of Ag colloid. (a–e) Correspond to sample A to E in Table 1.

process. It can be deduced that the influence of the proximity of the silane and amine groups on the morphology of Ag colloids might be important; the more proximal the reducing groups and ligating groups, the smaller the silver particle size and distribution. More importantly, using a relatively lower concentration of triethylsilane as the external reducing agent resulted in much smaller particles of Ag colloids (compared with samples C and D). A lower concentration of the reductant probably led to a much slower reduction rate of the reaction. This allowed the amine groups to coordinate with Ag atoms more effectively to prevent Ag from agglomeration to some degree. This demonstrated that the reduction rate was quite important for controlling the morphology of Ag colloids. This result was consistent with the outcomes that the Ag colloids made at 0 °C were much smaller and more narrowly distributed than the samples made at 25 °C (compared with samples B and E). It was easy to understand that either the mobility of the Ag atoms or the reduction rate of the reaction was expected to be much slower at a relatively lower temperature, which could generate smaller Ag colloids.

Apart from the TEM images, another measurement was also obtained to characterize the Ag colloids. Dynamic light scattering can provide information about the hydrodynamic diameters of the obtained colloids. The data are shown in Fig. 3; the data indicated that the average particle sizes of the colloids were 11.7, 1.9, 3.4, 3.9, and 6.1 nm for samples A–E, respectively, which exhibited the same trend as that observed in the TEM images. The data provided by dynamic light scattering reflected the particle size of the entire colloid in addition to that of the sole Ag particles. In other words, actually, the Ag particles were embedded in a shell of the functionalized oligomer. It was not surprising that the particle sizes determined by DLS were somewhat larger than those derived from the TEM images since the data from TEM represented the individual Ag particle size rather than that of the whole colloid.

UV-visible spectroscopy was performed as well to characterize the Ag colloids. As shown in Fig. 4, no distinct absorption peaks appear for the polymer shell in the visible region, while Ag colloids under a different preparation process exhibit a wide absorption band in the visible light region centered around 400–420 nm. This is the characteristic absorption for the surface plasmon resonance (SPR) peaks of Ag NPs.[33–36] For the

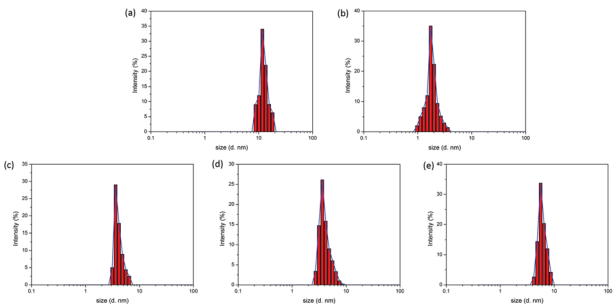

Fig. 3 DLS data for the Ag colloids. (a–e) Correspond to samples A to E in Table 1.

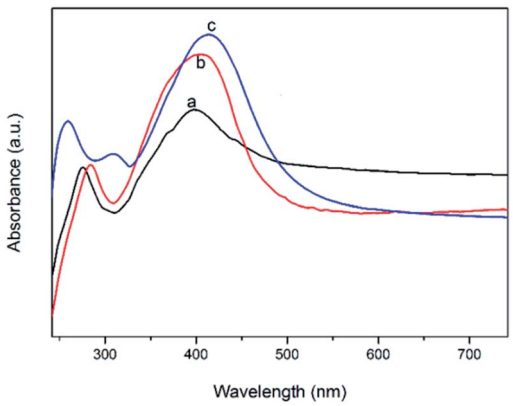

Fig. 4 UV-visible spectra of Ag colloid. (a–c) Correspond to samples B–D in Table 1.

sample B (spectrum a), the SPR peak at approximately 400 nm was the widest, indicating that the silver nanostructures were the smallest. The obvious red shift in the absorption band of Ag NPs (from a to c) indicated that the particle size gradually increased, causing the SPR peaks to narrow and increase in intensity.[37] These observations were consistent with the trends determined by TEM.

Ag XANES was performed to investigate the oxidation states of Ag by the intensity of a white line at the edge energy. Fig. 5 shows the XANES spectra of the silver colloids with the standard silver foil and silver nitrate. The silver nitrate absorption edge appeared at higher energy than that of the silver foil due to the oxidation state of Ag^{+}. Since the Ag atom in silver nitrate lost a "d" electron, the "1s" orbital electrons were deshielded from the nucleus; therefore, their binding energy increased.[38] The spectra obtained from samples B to D were very similar, and their absorption edges appeared at the same energy as that of the silver foil. No intense white line characteristic of $AgNO_3$ was observed. This information confirmed that the samples were completely reduced and that silver existed as Ag(0), which agreed well with the UV-vis results.

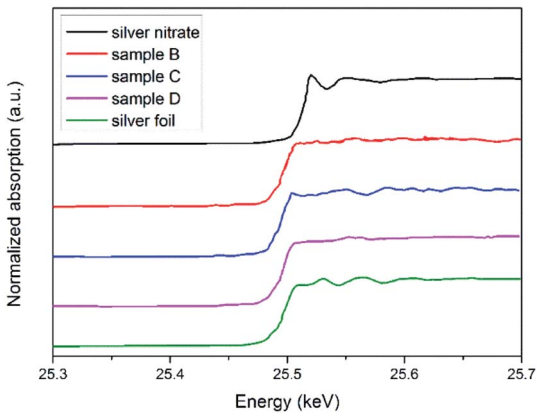

Fig. 5 Normalized absorption spectra at the Ag K-edge. From top to bottom, silver nitrate, sample B, sample C, sample D, silver foil (Ag^0), respectively.

Characterization of silica-supported Ag nanoparticles

The Ag colloid with the smallest particle size and the narrowest distribution (sample B) was prepared to synthesize supported Ag/SiO_2 nanoparticles. The colloidal particles were deposited onto silylated silica and calcined in He and O_3/O_2 at 150 °C, which could burn and get rid of all the organics and thus convert siloxane into SiO_2.[39] Among the samples, the Ag loadings were 1 wt%, 2 wt%, 3 wt%, and 4 wt%; the samples were denoted as Ag/SiO_2-1, Ag/SiO_2-2, Ag/SiO_2-3, and Ag/SiO_2-4, respectively.

XPS analysis was conducted to further elucidate the surface composition of the silica-supported Ag nanoparticles. For all the Ag/SiO_2 samples, there was no detectable Cl, N or S by XPS in any of the samples. The peaks with binding energies of 282.7, 530.3, 100.7 and 366.3 eV were attributed to C 1s, O 1s, Si 2p and Ag 3d, respectively, indicating the presence of the C, O, Si and Ag elements in the samples (Fig. S3†). Higher-resolution spectra were obtained to investigate the electronic states of the elements. In the spectrum of Ag 3d in Fig. 6, two peaks centered at 368.2 and 374.2 eV with a spin–orbit separation of 6 eV can be assigned to Ag $3d_{5/2}$ and Ag $3d_{3/2}$, respectively. These results further verified that only metallic Ag oxidation states were present in the supported Ag samples.[40] Furthermore, the intensity of Ag 3d increased with the increase in Ag loading, which was consistent with the results of our experiments.

The STEM images of Ag/SiO_2-1, Ag/SiO_2-2, Ag/SiO_2-3, and Ag/SiO_2-4 are shown in Fig. 7. The particle size of the Ag colloid used for the preparation of catalysts was 1.2 ± 0.4 nm, as shown in Fig. 2. The Ag particle sizes of the catalysts gradually increased from 1.9 nm to 3.5 nm as the silver loading increased from 1 wt% to 4 wt%. The reason was that the Ag particles in these samples were surrounded by siloxane oligomers and the silver loading increased as the organics increased. We had to remove the organics after the thermal treatment to achieve the Si–O–Si cluster around the Ag nanoparticles so as to prevent the Ag particles from agglomerating to some degree. During calcination, the organics served as the fuel to cause local heating. The initial growth of Ag clusters probably occurred within the same Ag-PMHS particle. With more organics being burnt and more overheating, collisions between particles occurred, where

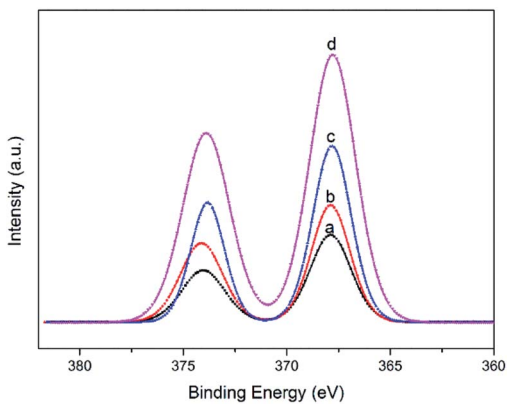

Fig. 6 XPS spectra of Ag 3d: (a–d) correspond to Ag/SiO_2-1, Ag/SiO_2-2, Ag/SiO_2-3, Ag/SiO_2-4.

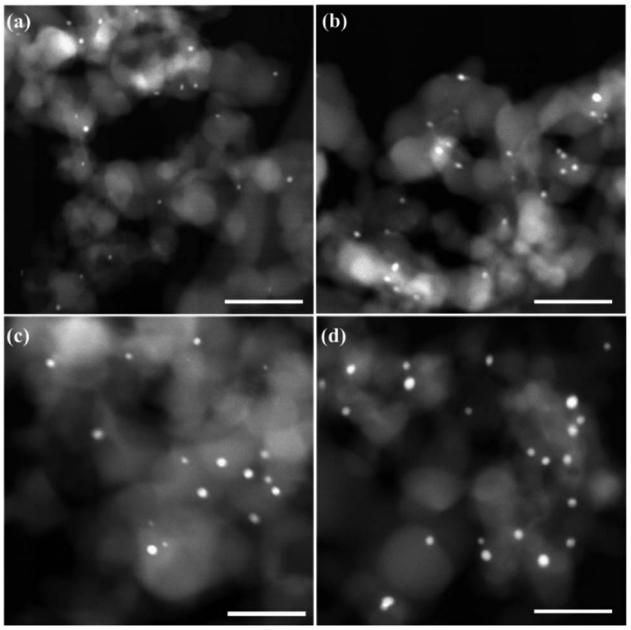

Fig. 7 STEM images of Ag/SiO_2. (a–d) Correspond to Ag/SiO_2-1, Ag/SiO_2-2, Ag/SiO_2-3, Ag/SiO_2-4. Scale bar is 20 nm.

interparticle exchange of Ag particles took place and this enabled their subsequent agglomeration. It can be concluded that the Ag particles prepared in this method were highly dispersed and were relatively stable under thermal conditions.

Catalytic performance of Ag/SiO_2 nanoparticles

The catalytic reduction of 4-NP in the presence of $NaBH_4$ was chosen as a model reaction to quantitatively evaluate the catalytic activity of the prepared Ag/SiO_2 samples. Although the reaction is thermodynamically favorable, it can hardly be triggered without catalysts. It has been widely applied to evaluate the catalytic activities of various metallic NPs.[41,42] The reaction can be monitored in real-time by UV-vis absorption spectroscopy. The 4-NP solution exhibited a strong absorption peak at 317 nm in neutral or acidic conditions. Upon the addition of the $NaBH_4$ solution, the characteristic peak of 4-NP immediately shifted from 317 to 400 nm (Fig. 8a), accompanied with a color change from light yellow to yellow-green due to the formation of the 4-nitrophenolate ions.[43,44] Notably, there was no change in the maximum absorption over time even after the superfluous addition of the $NaBH_4$ solution. The reduction of 4-NP did not occur without the use of Ag NPs as the catalysts. After the Ag/SiO_2-1 nanoparticles were added, the characteristic absorption peak of the 4-nitrophenolate ions at 400 nm gradually decayed, while a new peak at 295 nm, ascribed to the only product 4-AP, appeared (Fig. 8b). Meanwhile, the color of the 4-nitrophenolate ions gradually diminished within 10 min.

The concentration of $NaBH_4$ was supposed to remain constant during the entire reaction period. Owing to the excess amount of $NaBH_4$ in this reaction, pseudo-first-order kinetics based on 4-NP can be employed to calculate the reaction rate.[45] The linear relationship between $\ln(C_0/C)$ and the reaction time

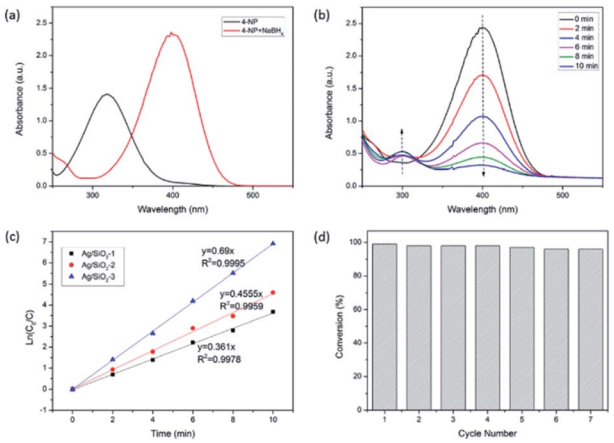

Fig. 8 The catalytic performance of the assembled Ag/SiO_2 NPs towards the reduction of 4-NP. (a) UV-vis spectra of the 4-NP solution after the addition of $NaBH_4$; (b) time-dependent UV-vis spectra of the reaction with Ag/SiO_2-1; (c) reaction rate plots using Ag/SiO_2 with different Ag loadings and different values of C_0, where C_0 is the initial concentration of 4-NP and C is the concentration of 4-NP at a particular time; catalyst dosage is 50 mg; (d) conversion efficiency of 4-NP for 7 successive reaction cycles.

was observed with different Ag loadings (Fig. 8c), which further confirmed the applicability of the pseudo-first-order kinetics. The first-order rate constants of Ag/SiO_2-1, Ag/SiO_2-2, and Ag/SiO_2-3 were calculated to be 0.361 min^{-1}, 0.455 min^{-1}, and 0.69 min^{-1}, respectively. This value of k was relatively higher than those reported in the literature using different supported Ag NPs prepared through different experimental protocols.[46] The electron transfer from the BH_4^- ions to the 4-nitrophenolate ions occurred *via* the surface of the metal nanoparticles.[47] A higher Ag loading meant more Ag-active surfaces, thus favoring the reaction.

Apart from the activity and kinetics, the stability and reusability of the as-prepared Ag catalyst were further examined. It was demonstrated that the catalytic performance of the as-synthesized supported Ag NPs was considerably stable without any obvious decay even after seven successive experimental runs (Fig. 8d). The preeminent catalytic performance and reusability could be due to the quite small and highly dispersed Ag NPs anchored on the silica support. The comparison of the TEM images and XPS spectra before and after seven recycles is shown in ESI (Fig. S4 and S5†). A comparison of the sample before and after the catalytic evaluation was made. It was observed that there was no obvious increase either in the structure or the properties of the reused catalyst. This indicated that the as-synthesized Ag/SiO_2 catalyst was stable and did not agglomerate considerably during the catalytic performance evaluation.

Conclusions

In summary, we developed a practical and simple strategy that did not require strong stabilizers (S and P) to synthesize silver colloids. The preparation process was controlled by functionalized siloxane oligomers that played dual roles in encapsulation with both ligating functionalities (–NH) and reducing functionalities (–SiH). This strategy was successfully employed to mediate the variation in silver colloids even those smaller than 2 nm. The variation of the ratios of the functional groups permitted us to define relevant synthesis parameters, for instance, the proximity of silane and amine, the extent of stabilization of the bifunctional ligands and the reaction rates of Ag reduction, which could determine the morphology of the resulting Ag colloids. The Ag colloids obtained by this method were very stable even after being deposited on silica and went through He and O_3/O_2 calcination to get rid of the organics. Efficient assembly and high-density dispersion of Ag particles ranging from 1.9 to 3.5 nm with narrow size distribution were achieved on the surface of silica. They exhibited a high performance in the catalytic reduction of 4-NP to 4-AP with conversion of 98% within 10 min in the presence of $NaBH_4$. Furthermore, the Ag nanoparticles were quite stable and exhibited excellent reusability for seven successive reaction cycles without obvious decay. Because the principles applied in this synthesis are general, the synthetic route can be applicable to synthesize many other late transition metal colloids with controllable morphology. Therefore, it can provide many promising applications in other fields such as in sensors, catalysis and antibacterial studies.

Conflicts of interest

There are no conflicts to declare in this paper.

Acknowledgements

This work was funded by the State Key Laboratory of Solidification Processing in NWPU (Grant No. SKLSP201816), Xi'an Science and Technology Bureau Innovation Leading Projects (Grant No. 201805037YD15CG21(23)) and China Postdoctoral Science Foundation (Grant No. 2018M643699).

Notes and references

1 L. Djerahov, P. Vasileva, I. Karadjova, R. M. Kurakalva and K. K. Aradhi, *Carbohydr. Polym.*, 2016, **147**, 45.
2 K. Esumi, R. Isono and T. Yoshimura, *Langmuir*, 2004, **20**, 237.
3 Z. Wang, E. Beletskiy, S. Lee, X. Hou, Y. Wu, T. Li, M. Kung and H. Kung, *J. Mater. Chem. A*, 2014, **33**, 1743.
4 V. K. Sharma, R. A. Yngard and Y. Lin, *Adv. Colloid Interface Sci.*, 2009, **145**, 83.
5 K. D. Hermanson, S. O. Lumsdon, J. P. Williams, E. W. Kaler and O. D. Velev, *Science*, 2001, **294**, 1082.
6 A. I. Lukman, B. Gong, C. E. Marjo, U. Roessner and A. T. Harris, *J. Colloid Interface Sci.*, 2011, **353**, 433.
7 T. Maneerung, S. Tokura and R. Rujiravanit, *Carbohydr. Polym.*, 2008, **72**, 43.
8 M. Maillard, S. Giorgio and M. P. Pileni, *J. Phys. Chem. B*, 2003, **107**, 2466.
9 G. Mcnay, D. Eustace, W. E. Smith, K. Faulds and D. Graham, *Appl. Spectrosc.*, 2011, **65**, 825.

10 W. Shen, Y. Qu, X. Pei, S. Li, S. You, J. Wang, Z. Zhang and J. Zhou, *J. Hazard. Mater.*, 2017, **321**, 299.
11 W. Zhang, F. Tan, W. Wang, X. Qiu, X. Qiao and J. Chen, *J. Hazard. Mater.*, 2012, **217–218**, 36.
12 C. Zhang, R. Zhang, S. He, L. Li, X. Wang, M. Liu and W. Chen, *Chemcatchem*, 2017, **9**, 980.
13 X. Wang, Z. Zhao, D. Ou, B. Tu, D. Cui, X. Wei and M. Cheng, *Appl. Surf. Sci.*, 2016, **385**, 445.
14 L. Yi, F. You, Y. Yuan, C. Yu, F. Cheng and S. C. Jiang, *J. Mater. Chem.*, 2012, **22**, 21173.
15 H. Hu, J. H. Xin, H. Hu, X. Wang, D. Miao and Y. Liu, *J. Mater. Chem. A*, 2015, **3**, 11157.
16 Y. Lei, F. Mehmood, S. Lee, J. Greeley, B. Lee, S. Seifert, R. E. Winans, J. W. Elam, R. J. Meyer and P. C. Redfern, *Science*, 2010, **328**, 224.
17 C. P. Joshi, M. S. Bootharaju, M. J. Alhilaly and O. M. Bakr, *J. Am. Chem. Soc.*, 2015, **137**, 11578.
18 K. H. Ng, A. H. Liu and R. M. Penner, *Langmuir*, 2000, **16**, 4016.
19 L. Lian, S. A. Mitchell, P. A. Hackett and D. M. Rayner, *J. Chem. Phys.*, 1996, **104**, 5338.
20 Z. Chen, Z. Wen and Q. Jiang, *J. Phys. Chem. C*, 2017, **121**, 3463.
21 O. S. Ivanova and F. P. Zamborini, *J. Am. Chem. Soc.*, 2010, **132**, 70.
22 H. Weller, *Angew. Chem., Int. Ed.*, 2010, **32**, 41.
23 L. Dai, W. You, E. Wang, S. Wu, Z. Su, Q. Du, Y. Zhao and Y. Fang, *Cryst. Growth Des.*, 2009, **9**, 2110.
24 J. A. Schuerman, F. R. Fronczek and J. Selbin, *Inorg. Chim. Acta*, 1989, **160**, 43.
25 P. C. Cheng, I. C. Liu, T. N. Hong, J. H. Chen, S. S. Wang, S. L. Wang and J. C. Lin, *Polyhedron*, 1996, **15**, 2733.
26 M. S. Bootharaju and T. Pradeep, Investigation into the reactivity of unsupported and supported Ag7 and Ag8 clusters with toxic metal ions, *Langmuir*, 2011, **27**, 8134.
27 D. V. Ozkan, S. Aydin, I. Hocaoglu, F. A. Yagci and N. Basaran, *Chem.-Biol. Interact.*, 2018, **291**, 212.
28 Y. Bhattacharjee, D. Chatterjee and A. Chakraborty, *Sens. Actuators, B*, 2018, **255**, 210.
29 H. Imai, A. Hitoshi Nakamura and T. Fukuyo, *Cryst. Growth Des.*, 2005, **5**, 1073.
30 C. H. Bartholomew, Mechanisms of catalyst deactivation, *Appl. Catal., A*, 2001, **212**, 17.
31 S. Kaserer, K. M. Caldwell, D. E. Ramaker and C. Roth, *J. Phys. Chem. C*, 2013, **117**, 6210.
32 H. Yoshida, T. Morishita, H. Fukushima, J. Ohshita and A. Kunai, *Org. Lett.*, 2007, **17**, 3367.
33 G. Shuang, Z. Zhang, K. Liu and B. Dong, *Appl. Catal., B*, 2016, **188**, 245.
34 T. P. Wallace, *The scattering of light and other electromagnetic radiation by Milton Kerker*, Academic Press, New York, 1969.
35 X. Wei, C. Shao, X. Li, N. Lu, K. Wang, Z. Zhang and Y. Liu, *Nanoscale*, 2016, **8**, 11034.
36 Z. Zhang, J. Huang, Y. Fang, M. Zhang, K. Liu and B. Dong, *Adv. Mater.*, 2017, **29**, 1606688.
37 D. L. Van Hyning, W. G. Klemperer and C. F. Zukoski, *Langmuir*, 2001, **17**, 3120.
38 J. L. Gardea-Torresdey, E. Gomez, J. R. Peralta-Videa, J. G. Parsons, H. Troiani and M. Jose-yacaman, *Langmuir*, 2003, **19**, 1357.
39 N. A. Mashayekhi, Y. Yi. Wu, M. C. Kung and H. H. Kung, *Chem. Commun.*, 2012, **48**, 10096.
40 M. Tahir, B. Tahir and N. A. S. Amin, *Appl. Catal., B*, 2017, **204**, 548–560.
41 K. Pushpavanam, S. Santra and K. Rege, *Langmuir*, 2014, **30**, 14095.
42 X. Zhang and Z. Su, *Adv. Mater.*, 2012, **24**, 4574.
43 M. Zhu, C. Wang, D. Meng and G. Diao, *J. Mater. Chem. A*, 2013, **1**, 2118.
44 J. Zhou, B. Duan, Z. Fang, J. Song, C. Wang, P. B. Messersmith and H. Duan, *Adv. Mater.*, 2014, **26**, 701.
45 S. Zhao, Y. Gao, J. Li, G. Zhang, R. Sun and C. P. Wong, *RSC Adv.*, 2015, **5**, 56974.
46 S. Lu, J. Yu, Y. Cheng, W. Qian, A. Barras, W. Xu, S. Szunerits, D. Cornu and R. Boukherroub, *Appl. Surf. Sci.*, 2017, **411**, 163–169.
47 G. Gahlawata and A. Choudhury, *RSC Adv.*, 2019, **9**, 12944.